THE CEBAF INJECTION LINE AS STERN-GERLACH POLARIMETER

R. Talman, LEPP, Cornell University; J. Grames, R. Kazimi, M. Poelker, R. Suleiman, Thomas Jefferson National Laboratory; B. Roberts, University of New Mexico

INTRODUCTION

It is explained how the CEBAF 123 MeV injection line can serve as one big Stern-Gerlach (S-G) polarimeter measuring the polarization state of the injected beam. No physical changes to the line are required and (though not optimal) beam position monitors (BPMs) already present in the line can be used to detect the S-G signals.

The historical Stern-Gerlach apparatus used a uniform magnetic field (to orient the spins) with quadrupole magnetic field superimposed (to deflect opposite spins oppositely) and a neutral, somewhat mono-energetic, unpolarized, neutral atomic beam of spin 1/2 particles. For highly-monochromatic, already-polarized beams produced by Jefferson Lab electron guns, the uniform magnetic field has become superfluous, and every quadrupole in the injection line produces polarization-dependent S-G deflection.

Starting from neutral silver atoms in the original experiment, for which the angular deflections were roughly $\Delta\theta^{Ag} \approx 0.0005$ radians, we can estimate the Stern-Gerlach deflections of relativistic electrons in the quadrupoles of a modern-day accelerator. In both cases the transverse force is due to the magnetic moment of a single electron. Magnets in the CEBAF beam line are much like the original (1923) Stern-Gerlach magnets. The transverse force is the same irrespective of whether the electron is free or a valence electron in the silver atom. An anticipated deflection of electrons with $\gamma_e = 12$ can be estimated from formulas for the angular deflection, $\Delta p_\perp/p_z$, for the ratio of force durations, v^e/v^{Ag}, and for the ratio of longitudinal momenta, p^{Ag}/p^e:

$$\begin{aligned}
\frac{\Delta p_\perp}{p_z} &= \text{Force}\frac{\text{duration}}{p_z} \\
\frac{v^e}{v^{Ag}} &= \frac{3\times 10^8}{10^3} = 3\times 10^5 \\
\frac{p^{Ag}}{p^e} &= \frac{M^{Ag}}{m_e}\,\frac{\gamma^{Ag}}{\gamma_e}\,\frac{v^{Ag}}{v^e} \\
&\approx \frac{106\times 2000 m_e}{m_e}\,\frac{1}{12}\,\frac{10^3}{3\times 10^8} \approx 0.05.
\end{aligned}$$

We therefore anticipate 6 MeV electron deflections of order

$$\Delta\theta^{6MeVe} \approx 0.0005 \times \frac{0.05}{3\times 10^5} \approx 10^{-10}\,\text{radians}.$$

With drift lengths being of order 1 meter, this suggests that the Ängstrom, which is equal to 10^{-10} m, is an appropriate unit for expressing the S-G betatron amplitudes to be expected.

For a dedicated reconfiguration of the beamline optics, the S-G deflection could be enhanced substantially. But, to minimize operational interuption, we first assume no beamline changes whatsoever, so that investigations can be almost entirely parasitic. Because the expected amplitudes are so small, we also consider reducing the beam energy to 6 MeV or less (from 123 MeV) throughout the line, by detuning the intermediate linac section, to increase the S-G effect.

Dual CEBAF electron beam guns produce superimposed 0.25 GHz (bunch separation 4 ns) electron beams for which the polarization states and the bunch phases can be adjusted independently. For example, the (linear) polarizations can be opposite and the bunch arrival times adjusted so that (once superimposed) the bunch spacings are 2 ns and the bunch polarizations alternate between plus and minus. The effect of this beam preparation is to produce a bunch charge repetition frequency of 0.5 GHz different from the bunch polarization frequency of 0.25 GHz. This difference will make it possible to distinguish Stern-Gerlach-induced bunch deflections from spurious charge-induced excitations.

Transverse bunch displacements produce narrow band BPM signals proportional to the f_r Fourier frequency components of transverse beam displacement. Because linac bunches are short there can be significant resonator response at all of the strong low order harmonics of the 0.25 GHz bunch polarization frequency. The proposed S-G responses are centered at odd harmonics, $f_r = 0.25, 0.75, 1.25$ GHz, but *not* at even harmonics, such as the 0.5 GHz bunch charge frequency. This greatly improves the rejection of spurious "background" bunch displacement correlated with bunch charge. For further background rejection the polarization amplitudes are modulated at a low, sub-KHz frequency which shifts the S-G response to sidebands of the central S-G frequencies.

STERN-GERLACH DEFLECTION OF A RELATIVISTIC PARTICLE

We are primarily interested in the Stern-Gerlach deflection caused by the passage of a point particle with velocity $v\hat{\mathbf{z}}$ and rest frame, transversely-polarized magnetic dipole moment vector $\mu_x^*\hat{\mathbf{x}}$, through a DC quadrupole, of length L_q, that is stationary in the laboratory frame K. The purpose of this section is to relate the Stern-Gerlach and Lorentz force deflections in a quadrupole in a transfer line such as the CEBAF injection line.

It is valid to formulate the calculation with an impulsive approximation, in which the integrated momentum imparted to a particle passing through a quadrupole is small enough to justify neglecting the spatial displacement oc-

curring during the encounter and keeping track of only the angular deflection.[1] One also notes the particle speed is conserved because it is only a longitudinal component of force that can change the particle speed. The Stern-Gerlach deflection in the electron's instantaneous rest frame can simply be copied from well-established non-relativistic formalism[1]; the transverse force is given by

$$F'_x = \mu^*_x \frac{\partial B'_x}{\partial x'}. \tag{1}$$

Following notation of Conte[2], the rest frame magnetic moment is symbolized by μ^* to stress that it is specific to the rest frame, irrespective of whatever reference frame is being discussed. As viewed in the K' rest frame, the passing magnet is Lorentz-contracted to length L_q/γ, the time spent by the particle in the magnetic field region is L'_q/v, and the integrated, rest frame transverse momentum impulse is

$$\Delta p'_x = F'_x \frac{L'_q}{v} = \frac{\mu^*_x}{v} \frac{\partial}{\partial x'} (B'_x L'_q). \tag{2}$$

To determine B'_x the laboratory magnetic field B_x needs to be Lorentz transformed to the moving frame K'. This produces both an electric and a magnetic field, but it is only the magnetic field that produces Stern-Gerlach displacement in the particle's rest frame. The Lorentz transformation yields[3] $B'_x = \gamma B_x$. We conclude that the product $B_x L_q = B'_x L'_q$ is the same in laboratory and rest frames. Since the displacement $x = x'$ and the transverse momentum component $\Delta p'_x = \Delta p'_x$ are also invariant for Lorentz transformation along the z axis, Eq. (2) becomes

$$\Delta p^{SG}_x = F_x \frac{L_q}{v} = \frac{\mu^*_x}{v} L_q \frac{\partial B_x}{\partial x}, \tag{3}$$

and similarly Δp^{SG}_y. The "SG" superscripts have been introduced to distinguish Stern-Gerlach deflections from Lorentz force deflections.

The conclusion so far is that formula (3), derived historically using non-relativistic kinematics, is valid even for relativistic particle speed. Of course, because v cannot exceed c, the transverse force saturates as the particle becomes relativistic. Since the particle momentum continues to increase proportional to γ, the S-G angular deflection in a fixed excitation quadrupole field falls as $1/\gamma$.

The magnetic field components of an erect DC quadrupole are given by

$$B_x = ky,\ B_y = kx, \quad \text{where } k = \frac{\partial B_x}{\partial y} = \frac{\partial B_y}{\partial x}, \tag{4}$$

and $|\partial B_x/\partial x| = |\partial B_x/\partial y|$. The quadrupole field in the original Stern-Gerlach experiment would, in modern accelerator terminology, be referred to as "skew". The strong quadrupoles in the CEBAF line under consideration are "erect". To simplify the paper we simply ignore this distinction, possibly introducing $\sqrt{2}$ errors in some formulas.

Treating a quadrupole of length L_q as a thin lens, the Lorentz force on a point particle of mass m and charge e traveling with velocity $v\hat{\mathbf{z}}$ through the quadrupole imparts momentum

$$\Delta \mathbf{p} = \mathbf{F}(x, y)\, \Delta t = eL_q k (y\hat{\mathbf{y}} - x\hat{\mathbf{x}}). \tag{5}$$

The relativistic longitudinal particle momentum of the particle is $p = \gamma m v$ and its (small) angular deflections are given by

$$\Delta\theta_x \hat{\mathbf{x}} + \Delta\theta_y \hat{\mathbf{y}} = \frac{\Delta \mathbf{p}}{p} = q_x x \hat{\mathbf{x}} + q_y y \hat{\mathbf{y}}, \tag{6}$$

where inverse focal lengths $q_x = 1/f_x$ and $q_y = 1/f_y$ of the quadrupole satisfy

$$q_x = -\frac{eL_q k}{p} = -\frac{L_q c \partial B_y/\partial x}{pc/e} = -q_y. \tag{7}$$

The Stern-Gerlach angular deflections are given by

$$\Delta\theta^{SG}_x = \frac{\Delta p^{SG}_x}{p} = \frac{\mu^*_x L_q k}{pv}, \tag{8}$$

and similarly for y. Comparing with Eqs. (7), one sees that the Stern-Gerlach deflection in a quadrupole is strictly proportional to the inverse focal lengths of the quadrupole;

$$\boxed{\Delta\theta^{SG}_x = -\frac{\mu^*_x}{ec\beta} q_x, \quad \text{and} \quad \Delta\theta^{SG}_y = \frac{\mu^*_y}{ec\beta} q_y,} \tag{9}$$

These formulas are boxed to emphasize their universal applicability to all cases of polarized beams passing through quadrupoles. For all practical cases $\beta \approx 1$.

As mentioned previously, the S-G deflection in a fixed excitation quadrupole magnet is proportional to $1/\gamma$. Yet, superficially, deflection formulas (9) show no *explicit* dependence on γ. This is only because the angular deflections are expressed in terms of quadrupole inverse focal lengths. For a given quadrupole at fixed quadrupole excitation, the inverse focal length scales as $1/\gamma$. This has the effect of "hiding" the $1/\gamma$ Stern-Gerlach deflection dependence, which is due to the proportionality to γ of the beam stiffness.

With μ^*_x and μ^*_y differing from the Bohr magnetron μ_B only by $\sin\theta$ and $\cos\theta$ factors respectively, a convenient physical constant for the evaluation is

$$\frac{\mu_B}{ec} = 1.932 \times 10^{-13}\,\mathrm{m}. \tag{10}$$

Numerically, Eq. (9) yields Stern-Gerlach-induced, Courant-Snyder betatron amplitudes proportional to

$$\sqrt{\beta_x}\, \Delta\theta^{SG}_x = -(1.932 \times 10^{-13}\,\mathrm{m}) \sqrt{\beta_x}\, q_x, \tag{11}$$

[1] For anomalous electron angular momentum $G = 0.00117$ the spin precession angle occurring during angular deflection $\Delta\theta$ of approximately $G_e \gamma \Delta\theta/(2\pi)$ is negligible. Also, the effect of non-zero electric field in the electron rest frame (obtained by Lorentz transformation of the quadrupole magnet at rest in the laboratory), can be included in the rest frame orbit equation and shown to be negligible.

and similarly for y. The $\sqrt{\beta}$ factor has been included because the transverse displacement Δx_j at downstream location "j" caused by angular displacement $\Delta\theta_i$ at upstream location "i" is given (in either plane) by

$$\Delta_j = \sqrt{\beta_j \beta_i}\, q_i \sin(\psi_j - \psi_i). \qquad (12)$$

where $\psi_j - \psi_i$ is the betatron phase advance from "i" to "j", and Δ_j stands for either Δx_j or Δy_j. Sample Δ_j-values for locations in the CEBAF injection line are listed in Tables 1 and 2.

The quadrupole deflection formulas just derived are next evaluated numerically for the CEBAF injection line.

BEAM LINE APPARATUS AND OPTICS

Beamline beta functions are shown in Figure 1. To facilitate the interpretation of S-G deflections the only points plotted are at the locations of quadrupoles, BPMs, or beam charge monitors (BCMs).

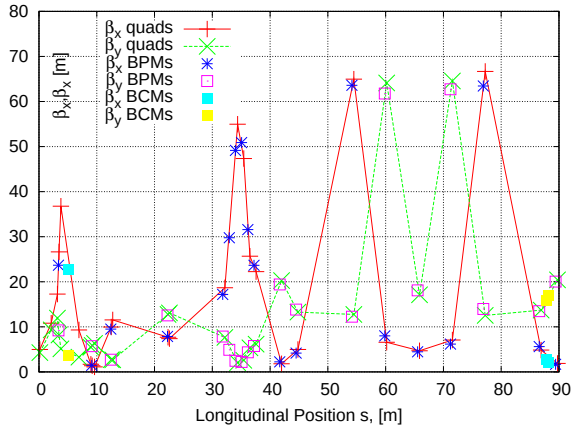

Figure 1: Beta functions for the current 123 MeV injection line optics. Points are plotted only at current quadrupole, BPM, and beam charge monitor (BCM) locations.

To illustrate the sort of calculattions required, the S-G signals to be expected at each BPM position during routine (alternating polarization) CEBAF 123 Mev electron injection line operation, are calculated for a "proof-of-principle" test. Once successful, this test should motivate the development of a passive (non-destructive) form of high analyzing power, precision polarimetry. Table 1 shows the integrated S-G responses at all available BPMs. These are phasor sums of the contributions from all quadrupoles upstream of the particular BPM. Table 2 gives the phasor contributions from individual quadrupoles for the case of just one of the BPMs, (IPM0R07).

S-G SPECIFIC BEAM PREPARATION

The smallness of the S-G signal, especially relative to spurious charge-sensitive cavity responses, makes it critical for the polarized beam to be prepared for maximum rejection of spurious background.

Table 1: Accumulated S-G betatron responses at all beamling BPMs. For one particular BPM, namely IPM0R07 spelled-out betatron contributions from its upstream quadrupoles are given in Table 2.

s m	BPM label	$\Re(a_x)$ Eq.(12)	$\Im(a_x)$	$\Re(a_y)$ Eq.(12)	$\Im(a_y)$	K MeV
3.38	IPM0L02	-0.15	-0.02	-0.15	-0.02	6
9.14	IPM0L03	-1.80	-1.16	-2.62	2.27	6
12.43	IPM0L04	6.41	0.63	1.57	-2.15	6
22.25	IPM0L05	-0.25	0.94	-1.32	-1.18	6
31.80	IPM0L06	1.89	1.47	1.55	-0.87	6
32.95	IPM0L06A	-0.24	1.70	0.45	0.19	6
34.01	IPM0L07	-2.04	0.99	-0.07	-0.11	6
35.08	IPM0L08	-1.79	-0.95	0.71	-0.48	123
36.14	IPM0L09	-0.02	-1.24	1.82	0.68	123
37.21	IPM0L10	0.56	-0.12	0.62	2.43	123
41.66	IPM0R01	1.90	-1.29	1.90	-4.25	123
44.50	IPM0R02	-1.05	4.58	1.41	3.16	123
54.17	IPM0R03	-9.12	-3.64	0.10	1.73	123
59.85	IPM0R04	-0.90	0.72	3.93	-3.46	123
65.54	IPM0R05	-7.51	-0.57	-2.92	-1.13	123
71.22	IPM0R06	-1.30	-0.07	-0.41	5.80	123
76.91	IPM0R07	-8.64	4.05	3.01	0.39	123
86.58	IPM0R08	0.33	-4.24	-1.33	4.52	123
89.41	IPM0R09	0.58	2.25	-2.83	-4.97	123

Table 2: . Individual betatron amplitude contributions from each listed quadrupole to a particular BPM (namely IPM0R07). The coherent sum of these amplitudes produces that BPM's accumulated amplitudes listed in Table 1.

quad label	$s_{\rm quad}$	$\Re(a_x)$	$\Im(a_x)$	$\Re(a_y)$	$\Im(a_y)$	K
MQJ0L02	3.19	0.33	-3.60	-0.04	0.47	6
MQJ0L02A	3.80	2.06	4.66	-0.17	-0.39	6
MQJ0L03	9.62	-0.27	0.17	-0.59	0.36	6
MQJ0L04	12.77	0.15	-0.00	0.02	-0.00	6
MQD0L06	32.17	-0.04	0.02	1.29	-0.65	123
MQB0L07	34.38	0.63	0.70	-0.10	-0.11	123
MQB0L08	35.44	0.92	-0.04	-0.68	0.03	123
MQB0L09	36.51	-0.80	1.09	1.16	-1.58	123
MQB0L10	37.58	-0.18	-0.68	0.25	0.93	123
MQD0R01	41.99	-1.13	-1.14	2.17	2.19	123
MQD0R02	44.82	0.00	-0.95	-0.00	0.87	123
MQD0R03	54.49	-5.24	1.02	1.75	-0.34	123
MQD0R04	60.18	0.11	0.53	-0.60	-2.79	123
MQD0R05	65.86	-5.43	1.27	-1.70	0.40	123
MQD0R06	71.55	0.25	0.99	0.25	0.99	123

Recent ILC-motivated BPM performance investigations [4][5][6][7] are relevant to our proposed Stern-Gerlach (S-G) detection experiment. Resonant beam position detection relies on two TM cavities. The charge-sensitive cavity (needed to normalize the charge) is tuned to resonate in a transversely symmetric mode at the bunch frequency. The position-sensitive cavity is tuned to resonate in a transversely asymmetric mode at the bunch frequency.

(By the Heisenberg uncertainty principle) it would not be feasible to locate a single mono-energy electron with usefully small transverse accuracy. This makes the electron charge e unnaturally small for present purposes. For comparison we define a "standard macro-charge" as the charge of $N_e = 10^{10}$ electrons, which is a typical number of electrons in each bunch in an ILC BPM prototype test. Classical (rather than quantum) mechanics is adequate for treating the centroid motion of such a large number of electrons,

even as regards their mean spin orientation.

A CEBAF beam is CW, with beam current of, say, 160 μA, which corresponds to a current of about 10^5 (just-defined) macro-charges per second. For S-G detection the Ångstrom is a convenient transverse length unit for S-G detection. For successful ILC operation the transverse beam positions need to be controlled to about ± 10 Å.

The bunch structures of the CEBAF injector (123 MeV, 160 μA, 0.5 GHz) and the Accelerator Test Facility (ATF) at the KEK laboratory (1.3 Gev, $N_e e = 10^{10} e$ macro-charge at 5 Hz pulse rate) are very different. We ignore the energy difference, which is thought to be unimportant for the comparison. For a typical cavity resonator quality factor of $Q_r = 10^4$ and frequency of 1 GHz, the cavity discharging time is far shorter than the ATF repetition period. This makes it appropriate to treat the ATF resonant response on a pulse-by-pulse basis. Essentially different in time structure, the CEBAF resonator response is continuous wave (CW) with the previously-defined macro-charges passing through the cavity at 100 kHz rate.

In a linac beam line, the fact that each bunch passes an S-G sensitive BPM only once, makes it hard to arrange for the polarization of successive bunches to be different. As already explained, high frequency bunch polarization modulation frequency is made possible by superposing staggered bunch trains having different polarizations. Figure 2 illustrate our planned, superimposed CEBAF bunch train. Bunches are labeled A in one of two pre-superimposed bunch trains and B in the other. Time domain plots are on the left, frequency spectra on the righ. The foreground S-G betatron signal oscillates at (harmonics of) 0.25 GHz, while the background charge signal oscillates at (harmonics of) 0.5 GHz. For resonant cavity BPMs the S-G detector would be tuned to a harmonic of the 0.25 GHz fundamental, for example to the third or fifth harmonic, for more convenient (smaller) cavity dimensions.

We assume the polarization of the superimposed A and B beams are also modulated with (low) frequency ω_m. The time domain, $i\,p(t)$ current-polarization products of the separate A and B beams are then given by

$$i\,p^A(t) = \sum_{n=-\infty}^{\infty} \delta(t - nT_0)(A + a\cos\omega_m t) \qquad (13)$$

$$i\,p^B(t) = \sum_{n=-\infty}^{\infty} \delta(t - T_0/2 - nT_0)(A - a\cos\omega_m t).$$

and are plotted on the left in Figure 2. The modulation amplitude a is drawn much smaller in magnitude than the unmodulated polarization amplitude A. But over-modulation, with values of a as great as $2A$, to maximize the side-band amplitudes, might be practical. There are two essential differences between the A and B beams. The beam pulses are shifted in time by one half cycle and the sign of the modulation is reversed. The modulation frequency ω_m, for which the frequency is expected to be in the range $0 < f_m < 1$ kHz, is exaggerated by many orders of magnitude in this figure, since $f_0 = 1/T_0$ is about 0.75 GHz. Champeney[9] gives the A-beam, cosine-modulated current-polarization Fourier transform $IP^A(\omega)$ to be

$$I\,P^A(\omega) = \sum_{n=-\infty}^{\infty} \frac{2\pi}{T_0}\left(A\delta\Big(\omega - n\frac{2\pi}{T_0}\Big) + \right. \qquad (14)$$

$$\left. + \frac{a}{2}\,\delta\Big(\omega - n\,\frac{2\pi}{T_0} + \omega_m\Big) + \frac{a}{2}\,\delta\Big(\omega - n\,\frac{2\pi}{T_0} - \omega_m\Big)\right).$$

The Fourier transform of the B-beam, sine-modulated, current-polarization Fourier transform is obtained by multiplying by the time-shift factor, $e^{-iT_0\omega/2}$ for which, when it is moved inside the summation, its ω factor can be replaced by $2\pi n/T_0$, due to the delta function having argument $\omega - 2\pi n/T_0$. The resulting $(-1)^n$ factor causes the sign alternation exhibited in the lower right graph in Figure 2. Because the modulation frequency is so low the corresponding time shift of the modulation is being neglected.

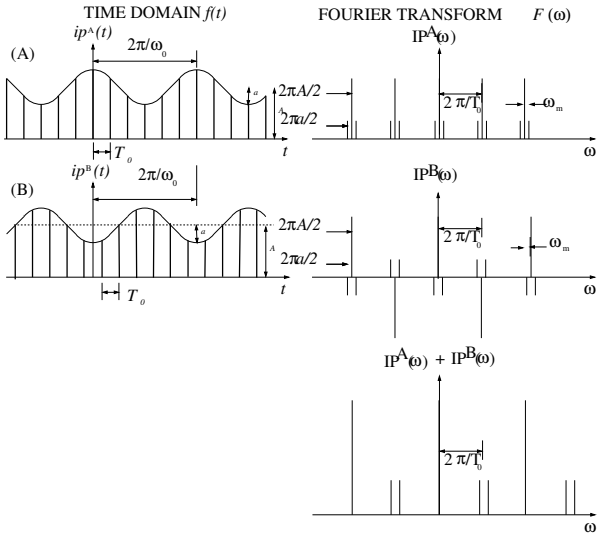

Figure 2: Time domain and frequency domain beam pulses for the A and B staggered, modulated-polarization beams. It is current-weighted polarization spectra that are plotted in these figures. The current spectra themselves are obtained by suppressing the modulation sidebands. In the A+B spectra the odd harmonics of beam current cancel, effectively doubling the fundamental current frequency from 0.25 GHz to 0.5 GHz. But the current-weighted polarization side bands survive as odd harmonics of 0.25 GHz.

SIGNAL LEVELS AND BACKGROUND REJECTION

According to Eqs. (9) the transverse displacement magnitude Δ at distance L downstream of a quadrupole of strength q is given by

$$\Delta = (1.932 \times 10^{-13}\,\mathrm{m})qL$$
$$\overset{\text{e.g.}}{\approx} (2 \times 10^{-13}\,\mathrm{m}) \times 1/\mathrm{m} \times 10\mathrm{m} = 0.02\,\mathring{A}. \qquad (15)$$

The installed CEBAF beam position monitors are "antenna BPM's", each consisting of four short (approximately 4 cm long), longitudinal, probe antennas, symmetrically-located azimuthally, within cylindrical beam tubes. Not themselves being narrow band, these BPMs are more noise-sensitive than resonant BPMs. But they have the important advantages of responding to both symmetric and anti-symmetric modes over large frequency range, for example at both 0.75 GHz and 1.0 GHz, with the responses easily separable by narrow band external filtering.

Barry[10] gives the transverse impedance of standard CEBAF BPMs to be $Z_\perp = 3800\,\mathrm{V/m}$. Taking $200\,\mu$A as a satisfactory beam current, the corresponding BPM power level would be

$$\begin{aligned} P &\approx (0.0002)^2 \times 3800 \times (0.02 \times 10^{-10}) \\ &= 3.0 \times 10^{-16}\,\mathrm{W} = -125\,\mathrm{dBm}. \end{aligned} \tag{16}$$

At room temperature the thermal noise in a 1 Hz bandwidth is given by

$$\begin{aligned} P_{\mathrm{noise}} = kT\Delta f &= (1.38 \times 10^{-23}\mathrm{J/K}) \times (293\,\mathrm{K} \times 1\,\mathrm{Hz} \\ &= 4.1 \times 10^{-21}\,\mathrm{W} = -174\,\mathrm{dBm} \end{aligned} \tag{17}$$

This calculation suggests that the S-G signal level will be large enough to be distinguishable from thermal noise.

A more serious impediment to S-G detection is spurious cavity response to bunch charge rather than to bunch polarization. We now review the procedures to be employed in distinguishing S-G signals from background.

Centered cavity. Conventional BPM beam centering relies on exact cavity centering for which, ideally, there is no direct charge excitation at the position mode frequency. Roughly speaking, the ILC BPM prototypes have so far achieved absolute transverse position reproducibility of ± 15 nm, for bunch to bunch variation of beam bunches containing $N_e = 10^{10}$ electrons. This is roughly an order of magnitude greater than (i.e. inferior to) their theoretical-minimum expected resolution of ± 1.8 nm. The authors (persuasively) ascribe their BPM performance short-fall primarily to error sources other than thermal noise, such as instrument imperfections or cross-talk from spurious, forbidden-mode response to bunch charge.

The "good news" to be drawn from the ILC ± 1.8 nm noise floor is that, with long time averaging, because of the high average CEBAF beam current, coherent betatron oscillation amplitudes as small as, say, 0.02 Å can be expected to emerge from thermal noise, even with room temperature cavities. The "bad news" is that there is little reason to suppose that cavity-centering S-G selectivity (relative to spurious background excitation) can be improved appreciably by increasing data collection times. Based on this estimate, an S-G induced betatron amplitude of 0.02 Å, though distinguishable from thermal noise in a single, carefully-centered, conventional resonant BPM, can be expected to be dwarfed by a background/foreground ratio of more than one thousand. This limitation is specific to the beam position and beam charge signals occurring at the same frequency, as in conventional beam position centering.

Accuracies as small as ± 20 Å should be achievable with centered transverse resonant BPMs. We are striving to measure betatron amplitudes 1000 times smaller. Mainly we need to make the case that rejection of spurious BPM signals caused by the beam charge (rather than the beam polarization) can be improved by three orders of magnitude compared to their influence on currently achievable transverse resonant BPM accuracy. The further selectivity improvement factors to be expected are surveyed next.

Disjoint polarization and charge frequencies. As explained earlier, the polarized beam will be tailored so that the bunch polarization and bunch charge frequencies are different. In this condition the BPM cavity is sensitive to polarization at one frequency (0.75 GHz) and to charge at a different frequency (such as 0.5, or 1.0 GHz). Ideally, the resulting frequency domain filtering will suppress the spurious background response by many orders of magnitude. More realistically, there will still be background response, for example due to the small Fourier component of charge excitation due to not-quite-cancelling beam A and beam B currents.

Empirical beam steering to null "common mode" BPM responses at both even and odd harmonics of 0.25 MHz (which would all vanish for ideal beam preparation) is especially useful for rejecting spurious background excitation. This cancels both off-axis background excitation at the fundamental beam charge frequency and charge-imbalance background "leakage" from even harmonics to odd harmonics, while preserving the foreground S-G response differentially in the odd harmonics.

One can expect significant background/foreground suppression from these common mode suppression and differential mode frequency domain filtering measures—perhaps three orders of magnitude.

Sideband shift of polarization frequency. As explained previously, the effect of low frequency modulation of the beam polarizations is to shift the S-G response to sidebands of the central cavity resonance. To the extent the beam currents are unaffected by this modulation, the sideband response will provide a pure S-G signal. In practice the beam currents will, in fact, also be weakly modulated which will allow some background signal to leak out to the side-band frequencies. Still one can expect significant background/foreground suppression—perhaps two orders of magnitude.

Multi-detector response modeling. Referring again to the BPM listing, one notes that foreground S-G response is being monitored, with various (well known) degrees of sensitivity, in both x and y planes at 19 BPM locations. The extent to which the beam charges are being low-frequency modulated at the gun can be parameterized with a few parameters, such as 4, the main one describing charge imbalance. Modulation of initial (low energy) beam angles will

also mimick S-G signals in individual BPMs. The corresponding betatron amplitudes are adiabatically damped by the subsequent acceleration, but they may remain significant. But there is no reason to suppose that the downstream sensitivity to starting beam conditions is correlated with S-G sensitivity. If true, any spurious side-band responses can be subtracted by a model fitted to match the total responses at all BPMs. Perhaps two orders of magnitude selectivity improvement can be achieved.

Lock-in signal detection. Though not mentioned previously, it is also true that the resonator responses will be coherent with the beam bunch frequency. By lock-in detection, the in-phase and out-of-phase S-G sideband deflections can be determined individually. As well as improving noise rejection, this can serve to corroborate the response model just described. Perhaps one more order of magnitude selectivity improvement can be achieved.

Multiplied together, the possibility of achieving eight orders of magnitude rejection of spurious background has been described. This seems conservatively greater than the required three orders of magnitude indicated earlier. Another factor of 6 improvement might be achieved by lowering the beam energy entering the transfer line from 6 MeV to 1 MeV. This would be satisfactory for an initial proof of principle, but would not be tolerable for eventual routine polarimetry during production CEBAF running.

REFERENCES

[1] J. Porter, R. Pettifer, and D. Leadly, *Direct demoonstration of the transverse Stern-Gerlach effect,* American Journal of Physics, **71**, 1103, 2003

[2] M. Conte, et al., *The Stern-Gerlach interaction between a traveling particle and a time varying magnetic field,* arXiv:physics/0003069v1 [physics.acc-ph], 2000

[3] J. Jackson, *Classical Electrodynamics,* 3rd edition, John Wiley, 1998

[4] Y. Inoue, et al., *Development of a high-resolution cavity-beam position monitor,* PRST-AB **11**, 062801, 2008

[5] S. Walston, et al., *Performance of a high resolution cavity beam position monitor system,* Nuclear Instruments and Methods in Physics Research A, 578, p1, 2008

[6] C.J. Swinson, *Development of Beam Position Monitors for Final Focus Systems at the International Linear Collider*, Oxford University PhD Thesis, 2010

[7] N.Y. Joshi, *Design and Analysis Techniques for Cavity Beam Position Systems for Electron Accelerators,* University of London PhD Thesis, 2013

[8] Siwon Jang et al., *Development of a cavity-type beam position monitor with high resolution for ATF2,* Proceedings of IPAC2013, Shanghai, China, 2013

[9] D.C. Champeney, *Fourier Transforms and Their Physical Applications,* Academic Press, 1973

[10] W. Barry, *A General Analysis of Thin Wire Pickups for High Frequency Beam Position Monitors,* CEBAF PR-90-024, 1990